High-resolution cavity ringdown spectroscopy of the jet-cooled propyl peroxy radical $C_3H_7O_2$

Gabriel M. P. Just,[a] Patrick Rupper,[a] Terry A. Miller*[a] and W. Leo Meerts[b]

Received 18th November 2009, Accepted 12th February 2010
First published as an Advance Article on the web 18th March 2010
DOI: 10.1039/b924323b

We have obtained high resolution, partially rotationally resolved, jet-cooled cavity ringdown spectra of the origin band of the $\tilde{A} \leftarrow \tilde{X}$ electronic transition of two of the five conformers (G_1G_2 and G_1T_2) of the normal propyl peroxy radical, $C_3H_7O_2$, as well as the G conformer of the iso-propyl peroxy radical isomer. This transition, located in the near infrared, was studied using a narrow band laser source ($\lesssim$250 MHz) and a supersonic slit-jet expansion coupled with an electric discharge allowing us to obtain rotational temperatures of about 15 K. All three spectra have been successfully fitted using an evolutionary algorithm approach with a Hamiltonian including rotational and spin-rotational terms. Excellent agreement with the experimental spectra was obtained by fitting seven molecular parameters in each of the ground and the first excited electronic states as well as the band origin of the electronic transition. These parameters are compared with the results from electronic structure calculations. This analysis confirms unambiguously the previous room-temperature conformer assignments that were based upon quantum chemistry calculations.

1. Introduction

For decades, peroxy radicals (RO_2) have been known to be key intermediates in atmospheric chemistry as well as in low temperature combustion, and their role has been discussed in several overview articles.[1–4] The ability to monitor the presence as well as the concentration of these key radicals would lead to a better understanding of the chemistry of gas phase reactions involving such reactive species.[5–7] Due to the stringent demands for sensitivity and selectivity, the diagnostic technique of choice is likely spectroscopic[8] for whose application a prerequisite is well understood spectra.

Typically, peroxy radicals have been routinely followed in kinetic studies by monitoring their very strong $\tilde{B}$–$\tilde{X}$ electronic transition which lies in the UV, centered near 240 nm.[9] However, this transition is not suitable for high-resolution studies due to the repulsive nature of the $\tilde{B}$ state,[10] resulting in a broad, structureless spectrum.[11] Moreover this transition lacks selectivity for the R group in the peroxy radical, RO_2, and eliminates the possibility of resolving vibrational, rotational, and fine structure. Therefore, we have shifted the high-resolution spectroscopic interest to the intrinsically sharp and well structured but much weaker $\tilde{A}$–$\tilde{X}$ transition located in the near-infrared (NIR), which was first observed by Hunziker and Wendt.[12]

Our group has studied open-chain alkyl peroxy radicals ranging from methyl peroxy (R = CH_3) to pentyl peroxy (R = C_5H_{11})[13–19] using room temperature cavity ringdown spectroscopy (CRDS). We demonstrated the convenience of the NIR electronic transition as a species selective, as well as an isomer and even conformer specific, diagnostic technique.[20] However, due to the population of rotational levels under room temperature conditions as well as the overlap of different conformer transitions in the larger alkyl peroxy radicals, high precision spectroscopic parameters, such as rotational and spin-rotational constants, which are highly useful for benchmarking quantum chemistry calculations, cannot be extracted from these spectra.

Other groups have also studied the smaller gas-phase peroxy radicals such as methyl and ethyl peroxy by a variety of techniques, including negative-ion photoelectron spectroscopy,[21] photoionization,[22] cw-CRDS in the NIR[23] and NIR absorption detected by time-of-flight mass spectroscopy,[24] but have similarly failed to obtain high precision molecular parameters characterizing the rotational and spin-rotational structure.

We recently developed an experimental apparatus that allows us to combine a high-resolution laser source[25] with a slit-jet-cooled CRDS setup,[26] and have successfully used it to record the rotationally resolved $\tilde{A}$–$\tilde{X}$ spectrum near 1.35 μm transition of the perdeuterated methyl peroxy radical, CD_3O_2,[27] as well as the two conformers of the proteo and deutero isotopologues of the G and T conformers of the ethyl peroxy radical.[28] The experimental spectra have been modeled using a Hamiltonian that includes the rigid body rotation of an asymmetric top and the spin-rotation interaction. In the case of the CD_3O_2 spectrum, a least squares fitting procedure was used to simulate the well resolved spectrum. On the other hand, due to the incompletely resolved structure, an evolutionary algorithm (EA) approach was used to analyze and simulate the $C_2H_5O_2$ spectra. For both methyl and ethyl

[a] *Laser Spectroscopy Facility, Department of Chemistry, The Ohio State University 120 W. 18th Avenue, Columbus Ohio 43210. E-mail: tamiller@chemistry.ohio-state.edu; Fax: +1 (614) 292-1948*
[b] *Radboud University Nijmegen Institute for Molecules and Materials, Heyendaalseweg 135 6525 AJ Nijmegen, The Netherlands*

peroxy, the studies resulted in the high precision determination of 15 molecular parameters characterizing the $\tilde{A}$ and $\tilde{X}$ electronic states.

Our recent CRDS studies of the $C_3H_7O_2$ radical under room-temperature conditions[14] directly identified 5 conformers of the n-propyl peroxy radical (G_1G_2, G_1T_2, T_1G_2, T_1T_2 and G'_1G_2) and both conformers of the iso-propyl peroxy radical (G and T). However, the conformer assignments were based only upon high level electronic structure calculations[15] and spectral congestion caused significant overlap between conformer bands and prevented resolving rotational constants or spin-rotation structure in the spectra.

This paper extends our previous work to obtain and analyze the $\tilde{A}$–$\tilde{X}$ spectra for several conformers and isomers of the propyl peroxy radical under jet-cooled conditions with a narrow band laser source. As in the ethyl peroxy study, we have found it of use to analyze and fit these spectra using the EA approach due to the partially resolved nature of the experimental spectra. Our analysis produces a set of high precision molecular parameters characterizing the $\tilde{A}$ and $\tilde{X}$ states which we compare with the results of electronic structure calculations for these radicals.

2. Experimental

Our high-resolution CRDS experimental setup has been described in previous papers[26,27] so we will only give a brief summary of the aspects that are particularly relevant to this work. The 1.3 μm NIR radiation was obtained from the first Stokes of the stimulated Raman scattering (SRS) created by focusing the output of a pulsed (20 Hz), nearly Fourier-transform-limited (15 ns pulses), tunable, high energy ($\leq$100 mJ/pulse) Ti:Sapphire (Ti:Sa) laser source[25] into a stainless steel (1 m long) cell pressurized with typically 10 atm of H_2. The bandwidth of the NIR SRS radiation, due to pressure broadening, is estimated to be of the order of $\sim$200 MHz (FWHM), resulting, when combined with the residual Doppler broadening in the slit-jet expansion, in an instrumental linewidth of $\sim$250 MHz in the 1.3 μm region of the electromagnetic spectrum. The pulsed NIR radiation ($\sim$1 mJ) is coupled into the CRDS cavity, which consists of two high reflectivity mirrors (Advanced Thin Films, Colorado, USA, with reflectivity >99.999%) mounted on the arms of an evacuated chamber (0.67 m long). The mirrors are purged by a flow of inert gas argon to prevent a deposit from the reactive species onto the mirror surface.

The propyl peroxy radicals, $C_3H_7O_2$, are produced by expanding a mixture of $\sim$1% 1-propyl iodide (for the n-$C_3H_7O_2$) or 2-propyl iodide (for the iso-$C_2H_7O_2$) and $\sim$10% oxygen (O_2) in first run neon (75% Ne, 25% He) through a slit-jet (1 mm × 5 cm) nozzle (opening time 1 ms) and a pulsed discharge (10 Hz, 9 mm plasma channel length, 1 mm spacing between the electrodes). A high voltage is applied to the two stainless steel electrodes for $\sim$200 μs during the gas pulse, resulting in plasma currents of $\sim$300–400 mA. The precursor gas mixture is prepared by bubbling $\sim$500 Torr of an O_2 and Ne gas mixture through a sample bomb containing C_3H_7I at −45 °C.

The SRS radiation beam is used to probe the cooled supersonic gas expansion 10 mm downstream from the throat of the expansion where the radical concentration is estimated to be $\sim 5 \times 10^{12}$ molecules cm^{-3}.[27] Light emanating from the rear high reflector was detected by an InGaAs detector whose output was coupled to a 12-bit acquisition card in a computer running a LabView program created for the apparatus. Ringdown times of up to 250 μs and an experimental sensitivity of 0.02 ppm/pass (corresponding to a noise equivalent absorption of 4.5 ppb $Hz^{-1/2}$) have been achieved using our best mirror set.

The spectra were recorded using frequency scans of $\sim$10 GHz segments with a frequency step size of 50 MHz with 4 laser shots averaged at each frequency point. Each segment is linearized using a simultaneously recorded Fabry-Perot etalon trace (FSR $\approx$1 GHz). Absolute calibration was achieved by using the residual water absorption present in our vacuum chamber and by matching the lines with the water transitions reported in the HITRAN database.[29]

3. Theory

All the spectra of the propyl peroxy radical that have been recorded involve the 0_0^0 band of the $\tilde{A}$–$\tilde{X}$ electronic transition. Due to the fact that the radical is in a doublet state we expect both an observable rotational and spin-rotation structure in the spectra, but we expect hyperfine splittings to be unresolvable. Hence, the structure of each vibronic level is described by a Hamiltonian, $\mathscr{H}_T$,

$$\mathscr{H}_T = \mathscr{H}_{\mathrm{Rot}} + \mathscr{H}_{SR} + T_0(i) \quad (1)$$

where $T_0(i)$ is the energy of the vibronic state (vibrationless level of $\tilde{A}$ or $\tilde{X}$ electronic state) with $i = \tilde{A}$ or $\tilde{X}$ and $T_0(\tilde{X})$ is taken as zero.

We can express the rotational Hamiltonian, $\mathscr{H}_{\mathrm{Rot}}$, in the principal axis system as

$$\mathscr{H}_{\mathrm{Rot}} = AN_a^2 + BN_b^2 + CN_c^2 \quad (2)$$

where A, B and C denote, by convention, the rotational constants of the radical. The matrix elements of the rotational Hamiltonian, $\mathscr{H}_{\mathrm{Rot}}$, are well-known.[30,31]

The spin-rotation Hamiltonian has long been studied and derived by many authors[30,32–36] and can be written as,

$$\mathscr{H}_{\mathrm{SR}} = \frac{1}{2}\sum_{\alpha,\beta} \varepsilon_{\alpha\beta}(N_\alpha S_\beta + S_\beta N_\alpha) \quad (3)$$

where $\varepsilon_{\alpha\beta}$ represents the different components of the spin-rotation tensor expressed in the same principal axis system. It has been shown by several authors[32,37,38] that the components of the spin rotation tensor, $\varepsilon_{\alpha\beta}$ have first and second order contributions and the latter dominates.

In principle the spin-rotation tensor contains nine parameters. Brown and Sears have shown[37] that for molecules with C_1 point group symmetry, which is the point group symmetry of the observed radical spectra (see below for details), only six out of nine parameters could be determined independently from an experimental spectrum, and only

4 for C_s symmetry. A convenient way to express the tensor components is *via* their irreducible tensor combinations,

$$T_0^0(\tilde{\varepsilon}) = \frac{-1}{\sqrt{3}}(\tilde{\varepsilon}_{aa} + \tilde{\varepsilon}_{bb} + \tilde{\varepsilon}_{cc}) = \sqrt{3}a_0 \quad (4)$$

$$T_0^2(\tilde{\varepsilon}) = \frac{-1}{\sqrt{6}}(2\tilde{\varepsilon}_{aa} - \tilde{\varepsilon}_{bb} - \tilde{\varepsilon}_{cc}) = \sqrt{6}a \quad (5)$$

$$T_{\pm1}^2(\tilde{\varepsilon}) = \mp[(\tilde{\varepsilon}_{ba} + \tilde{\varepsilon}_{ab}) \pm i(\tilde{\varepsilon}_{ca} + \tilde{\varepsilon}_{ac})] = \pm(d \pm ie) \quad (6)$$

$$T_{\pm2}^2(\tilde{\varepsilon}) = [(\tilde{\varepsilon}_{bb} - \tilde{\varepsilon}_{cc}) \pm i(\tilde{\varepsilon}_{bc} + \tilde{\varepsilon}_{cb})] = b \pm ic \quad (7)$$

where the $\tilde{\varepsilon}_{\alpha\beta}$ are the reduced tensor components of Brown and Sears[37] and where the spin rotation parameters, a_0, a, b, c, d and e, were introduced by Raynes[33] and are used in our numerical analysis. In the current analysis, only the non-imaginary components of the spin-rotation tensor are included (see below for details).

We use a case (b) like basis due to the fact that we are expecting the spin-rotation coupling to be fairly small. We also use a prolate symmetric top representation, $|JNKSM_J\rangle$ in which the rotational angular momentum, **N**, and the spin-angular momentum, **S**, are coupled to generate the resultant total angular momentum, **J**. The M_J quantum number represents the projection of **J** on the space fixed Z axis and K denotes the projection of **N** on the a principal axis.

4. Spectral analysis and simulation

Previously, our group has used the approach of a least square fitting (LSF) procedure, employing the SpecView software package,[39] in order to obtain molecular parameters from a high resolution spectrum. This approach is traditional and appropriate if one has a well resolved spectrum for which individual line assignments are possible.

Recently, we have found that for partially resolved experimental spectra such as the ethyl peroxy radical,[28] the LSF approach is not suitable due to the nearly impossible task of assigning spectral features to given transitions. Under such circumstances the use of an EA[40] approach has been found preferable for spectral analysis and we adopt this approach for the present analysis.

4.1 Fitting with an evolutionary algorithm approach

The EA method is based upon the Darwinian theory of a natural selection process occurring by reproduction and mutation of genes in a chromosome leading to only best adapted individuals. From a spectroscopic point of view, the EA approach reproduces this behavior to fit an experimental spectrum with a model based upon the differences of the eigenvalues of the Hamiltonian, such as $\mathscr{H}_T$ given by eqn (1). The use of the EA approach to analyze the spectra of RO_2 has been illustrated in our recent work on ethyl peroxy[28] wherein further details are discussed.

In the present work the chromosome is composed of 18 genes corresponding to the 18 parameters that describe our spectra. These 18 parameters include the 15 total molecular parameters of $\mathscr{H}_T$, *i.e.* 3 rotational and 4 spin-rotational constants (imaginary terms omitted—see below) for each of the ground and first electronic states and the band origin (T_{00}), as well as the rotational temperature (T_R), and the two angles, θ and ϕ, describing the orientation of the electric dipole moment, μ, with respect to the principal axis system.

During the initial step of the fit, values for all the parameters are randomly set between the upper and lower limits input by the user. The next generation of chromosomes is generated from the selected best parent(s), which are determined by their fitness function using an evolution strategy (ES)[41–44] with mutative step size control. The number of individuals in a generation and the number of parents used to generate the next generation is determined by the choice of the algorithm and is discussed in detail in references 41–44.

The quality of the agreement between an experimental spectrum and its simulation is measured by a fitness function, F_{fg}:

$$F_{fg} = \frac{\sum_{r=-l}^{l} w(r) \sum_{i=1}^{N} f(i)g(i+r)}{\sqrt{\sum_{r=-1}^{l} w(r) \sum_{i=1}^{N} f(i)f(i+r)} \sqrt{\sum_{r=-l}^{l} w(r) \sum_{i=1}^{N} g(i)g(i+r)}} \quad (8)$$

The function $w(r)$ is called the overlap function which controls the sensitivity of the fitness function for a shift of the experimental and simulated spectra relative to each other. A more detailed explanation of the choice of $w(r)$ and l is given in a previous paper.[28]

If one wants to look at both spectra as vectors of dimension N (where N denotes the frequency points), then the numerator of F_{fg} is a weighted dot product[45] of these vectors and the denominator is simply a normalization factor, *i.e.*

$$F_{\mathrm{fg}} = \frac{(\boldsymbol{f}, \boldsymbol{g})}{\|\boldsymbol{f}\|\|\boldsymbol{g}\|} \quad (9)$$

In this expression, f represents the experimental spectrum while g represents the simulated spectrum.

The EA is very suitable for parallel computation. The calculations were performed on a Linux cluster in Nijmegen based on SUN Fire X4100 and X4150 machines. Typically 32 CPUs were used. Convergence occurs in approximately 300 generations corresponding to a wall clock time of about 35 min. The choice of the number of generations has been discussed in a previous paper.[28] In order to achieve fast convergence, a wise choice for the initial ranges of the different parameters in $\mathscr{H}_T$ is needed. We have found,[28] and see below, that if one wants to obtain an excellent first estimate of the rotational constants for both $\tilde{X}$ and $\tilde{A}$ states that good agreement between experiment and theory is obtained with output from an MP2(FULL)/6-31g(d) method and basis set. Therefore we used the molecular parameters from this calculation and set a search range of $\pm0.25\%$ as a starting point. The same procedure was done iteratively until convergence was obtained. To avoid any error in the fitting procedure (*i.e.* converging to a local minimum) several steps have been performed. For all the optimized geometries of every conformer and isomer of the propyl peroxy radical, a frequency calculation has been performed to ensure that the

geometry calculated was indeed the global minimum of the given conformer or isomer (*i.e.* no imaginary frequencies). Also we performed several fits with initial guesses up to 50% away from the calculated rotational constants. We observed a convergence to the fit values presented in this study. This was done to confirm that our fits were converging to the global minimum and not to any other possible local minimum. For the spin-rotation constants we used the procedure described in the next section to estimate their values and assumed a search range of predicted value times $10^{\pm 1}$.

5. Electronic structure, calculations and molecular parameter estimation

Both to obtain initial estimates for the molecular parameters and ultimately to benchmark experimental quantum chemistry calculations, we have performed a set of calculations for both electronic states of the radicals using various electronic structure methods and basis sets. Using the Gaussian 03 software package,[46] we computed the global minima for each observed conformer and isomer of the propyl peroxy radical for both ground, $\tilde{X}$, and first excited, $\tilde{A}$, electronic states, under the assumption that the observed spectra are in agreement with the previous room temperature conformer assignments.[15] The methods and basis sets include the density functional theory (DFT) method (B3LYP) with a 6-31+g(d) basis set which represents a fairly inexpensive calculation. We also used a full second order Møller–Plesset perturbation calculation (MP2 (FULL)) with a 6-31g(d) basis set. The final method used was the coupled cluster singlet and doublet, CCSD, with a 6-31+g(d) basis set. This is a somewhat more computationally expensive method and would be of considerable interest to benchmark. For the components of the dipole moments, we turned to a configuration interaction singles, CIS, method with a 6-31g + (d) basis. We performed the calculation at the optimized $\tilde{X}$ state geometries found by each the CCSD, B3LYP, and MP2 methods. It has to be noted that all the corresponding rotational constants have been calculated for the equilibrium geometry and not for the experimentally observed vibrationless level. However, since zero-point corrections for rotational constants are typically less than a few tenths of a percent, this only mildly affects comparison between the calculated and observed values. Table 1–4 summarize the rotational constants and T_{00} values calculated *via* the different electronic structure calculations.

In order to predict the values of the spin-rotational constants, we employ a semi-empirical approach described previously.[47] The basic physical requirement for this approach is that the electronic transition is localized on a given chromophore with common electronic structure for all the family members. Hence, the change of size of the carbon chain linked to this chromophore and its orientation will simply re-orient the principal inertial axes and change the values of tensor components expressed along them but leave unchanged the spin-rotational tensor components expressed in a local axis system tied to the chromophore.

A convenient local frame for the peroxy radicals has the z axis along the O_2 bond with x and y coinciding with the p orbitals perpendicular to it. If U is the unitary transformation relating the local and principal axes system then[28]

$$\tilde{\varepsilon}_S = I_S{}^{-1} U_S{}^{-1} U_R I_R \tilde{\varepsilon}_R U_R{}^{-1} U_S \qquad (10)$$

where $\tilde{\varepsilon}_S$ is the spin-rotation tensor of the molecule of interest expressed in its principal axis system. Both the I and the U matrices are dependent solely upon the geometry of the molecule and hence can be calculated from the optimized geometry of the electronic structure calculation. We use the spin-rotation tensor, $\tilde{\varepsilon}_R$, experimentally determined for CD_3O_2, as the reference molecule, to calculate $\tilde{\varepsilon}_S$ for $C_3H_7O_2$.

6. Experimental results

The propyl peroxy radical is the smallest alkyl peroxy that not only possesses multiple conformers, but also two different isomers. We first consider 1-propyl peroxy and then 2-propyl peroxy.

6.1 The 1-propyl peroxy radical

As mentioned previously, 1-propyl peroxy radical has 5 different conformers, see Fig. 1, that are expected to be populated under room temperature conditions; however, under jet cooled conditions ($T_R \approx 15$ K, $k_B T_R \approx 10$ cm^{-1}), this would not be the case assuming equilibrium exists between the rotational and conformer degrees of freedom. Tarczay *et al.*[15] calculated the ground state relative energy of all these conformers and assuming equilibrium only two conformers would be significantly populated, *i.e.* the most stable G_1G_2 conformer and the G_1T_2 conformer which lies only 27 cm^{-1} above the G_1G_2. The other 3 conformers are located more than $\gtrsim 100$ cm^{-1} above G_1G_2 and hence are not expected to be observed. There is evidence from other works on jet-cooled radicals that equilibrium in the conformer degree of freedom is probably not completely reached. Nonetheless, conformations with energies well above kT_R are usually not observed.[48] Indeed, we have been able to record resolved spectra for two sub-bands of the $\tilde{A}$–$\tilde{X}$ transition. The strongest band lies quite close to the unresolved contour assigned to the G_1G_2 conformer in the room-temperature spectrum, while the other band is close to the putative G_1T_2 assignment. We therefore take these assignments as our starting point recognizing that their confirmation or not will depend upon the qualitative agreement or disagreement between the rotation constants determined experimentally and those from electronic structure calculations.

6.1.1 The G_1G_2 conformer of n-$C_3H_7O_2$. We were able to record the spectra of the putative G_1G_2 conformer with a good signal to noise ratio (S/N $\approx$ 25 for the strongest spectral features). As Fig. 2 shows, the band spread over about 10 cm^{-1} and appears to be relatively highly congested due to the population of many rotational as well as spin rotational levels even at 15 K. This congestion renders assignments of individual spectral features to unique quantum-state defined transitions nearly impossible. Due to this inability to assign individual lines, the use of the LSF method to simulate the experimental spectrum is inappropriate. We therefore used the EA approach, whose description can be found in section 4.1, to simulate the spectrum and determine the most accurate

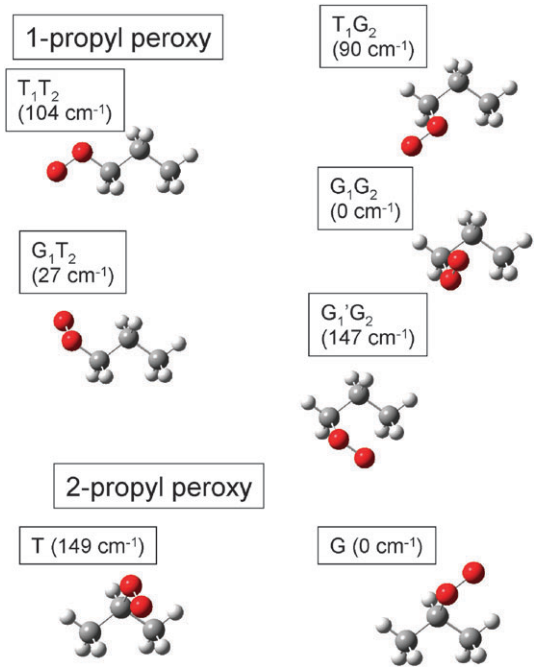

Fig. 1 Representations of the different isomers and conformers of the propyl peroxy radical. The numbers in parentheses represent the relative energy[15] of the conformers in the ground electronic state calculated by Tarczay *et al.*

values for the molecular parameters contained in $\mathscr{H}_T$ (eqn (1)) for both ground and first excited electronic states.

The resulting constants are summarized in Table 1. The converged result of the EA not only produces the best values for the fitted constants but at the same time assigns quantum numbers for individual transitions. This allows a classical least-squares fit using the assigned frequencies. In Meerts and Schmitt[40] this is called an assigned fit, and the definitions of the statistical errors and correlation coefficients are discussed in Appendix B of that paper. The errors reported in Table 1 are based on a 0.01 cm^{-1} uncertainty in the experimental line positions. The best agreement between the experimental spectrum and the fit was obtain with a rotational temperature of 15 K and a Voigt profile with a fixed Gaussian component of 250 MHz[27] and 1450 MHz Lorentzian width. The nature of such a large Lorentzian component of the linewidth is presently being studied and will be discussed in later reports.

The components of the transition dipole along the principal axes given in Table 1 are determined from the fit values of θ and ϕ using the relationships,

$$\mu_a = \mu \sin\phi \cos\theta \quad (11)$$

$$\mu_b = \mu \sin\phi \sin\theta \quad (12)$$

$$\mu_c = \mu \cos\phi \quad (13)$$

Fig. 2 shows both the overall spectrum (bottom) as well as a portion (top) of the resulting simulation and experimental trace. It appears obvious that the simulation and the experimental spectra are virtually identical. Table 1 shows that

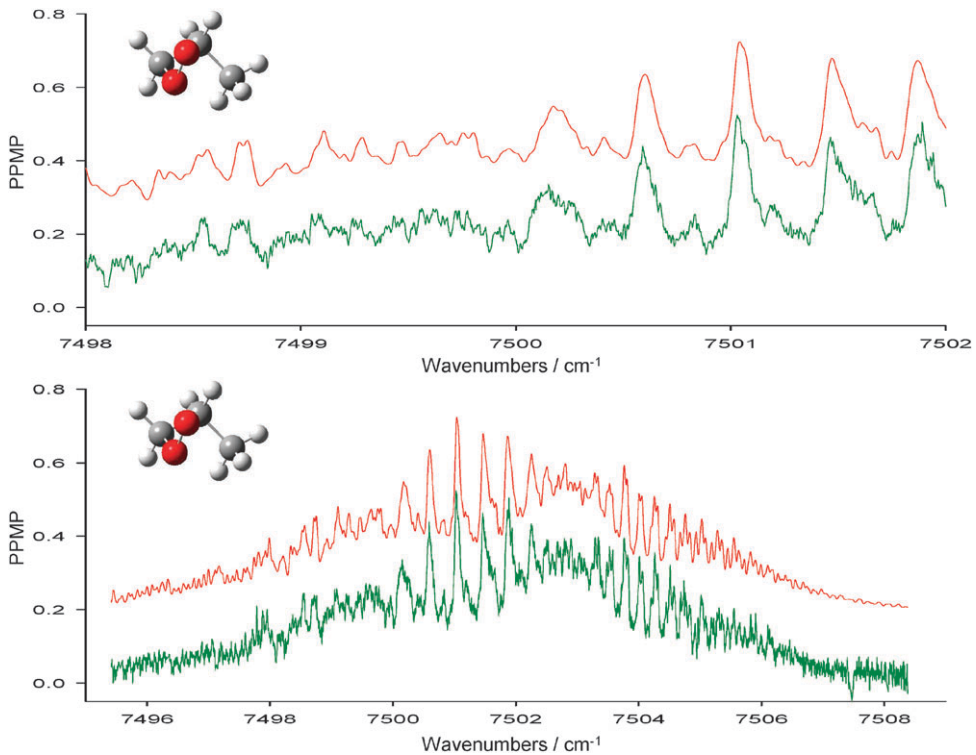

Fig. 2 Experimental and simulated spectra of the G_1G_2 conformer of the n-$C_3H_7O_2$ radical. The upper panel shows an enlargement of a 4 cm^{-1} section of the lower panel. In each panel, the top red trace is the simulated spectrum, using the fitted constants in Table 1, shifted upward by 0.2 PPMP (parts per million per pass) while the bottom green trace is the experimental spectrum. The vertical axis gives the absolute absorption in PPMP as a function of laser frequency along the horizontal axis.

Table 1 Molecular parameters of G_1G_2 conformer of n-$C_3H_7O_2$ radical from the experimental spectrum, with estimated errors in parentheses, and from the indicated electronic structure calculations (see text for details). The calculated T_{00} has been corrected by the scaled[49] ZPE correction under the harmonic oscillator assumption. The numbers in square brackets represent the percentage of error of the predicted constant with respect to the fitted results. The calculated and predicted constants are for the equilibrium geometry. The components of the transition moment are computed using the CIS method using the optimized geometries indicated

Const./cm^{-1}	Fit[a]	MP2(FULL)\6-31+g(d)	CCSD\6-31+g(d)	B3LYP\6-31+g(d)
A''	0.32199 (3)	0.32174 [0.078 (9)]	0.32078 [0.376 (9)]	0.33063 [−2.683 (9)]
B''	0.10725 (2)	0.10809 [−0.783 (19)]	0.10568 [1.464 (19)]	0.10205 [4.848 (19)]
C''	0.10007 (2)	0.10040 [−0.330 (20)]	0.09858 [1.489 (20)]	0.09576 [4.307 (20)]
$\tilde{\varepsilon}_{aa}'' = -(a_0 + 2a)''$	−0.0057 (5)	−0.0062 (15) [−9. (9)]	−0.0064 (15) [−12. (9)]	−0.0073 (15) [−28. (9)]
$\tilde{\varepsilon}_{bb}'' = (a + b - a_0)''$	−0.0012 (5)	−0.0017 (14) [−42. (42)]	−0.0016 (14) [−33. (42)]	−0.0015 (14) [−25. (42)]
$\tilde{\varepsilon}_{cc}'' = (a - b - a_0)''$	−0.0057 (5)	−0.0050 (15) [12. (9)]	−0.0049 (15) [14. (9)]	−0.0047 (15) [18. (9)]
$(1/2)(\tilde{\varepsilon}_{ab} + \tilde{\varepsilon}_{ba})'' = d''$	−0.0040 (10)	−0.0033 (22) [17.5 (25)]	−0.0033 (22) [18. (25)]	−0.0032 (22) [20. (25)]
$(1/2)(\tilde{\varepsilon}_{bc} + \tilde{\varepsilon}_{cb})'' = c''$	—	0.0009	0.0009	0.0007
$(1/2)(\tilde{\varepsilon}_{ac} + \tilde{\varepsilon}_{ca})'' = e''$	—	0.0040	0.0040	0.0044
A'	0.30300 (3)	0.30243 [0.188 (10)]	0.30039 [0.861 (10)]	0.30827 [−1.739 (10)]
B'	0.11047 (2)	0.11137 [−0.815 (18)]	0.10906 [1.276 (18)]	0.10547 [4.526 (18)]
C'	0.10219 (2)	0.10286 [−0.656 (20)]	0.10089 [1.272 (20)]	0.09772 [4.374 (20)]
$\tilde{\varepsilon}_{aa}' = -(a_0 + 2a)'$	0.0069 (5)	0.0050 (15) [28. (7)]	0.0051 (15) [26. (7)]	0.0061 (15) [12. (7)]
$\tilde{\varepsilon}_{bb}' = (a + b - a_0)'$	0.0022 (5)	0.0024 (14) [−9. (23)]	0.0024 (14) [−9. (23)]	0.0022 (14) [0. (23)]
$\tilde{\varepsilon}_{cc}' = (a - b - a_0)'$	0.0040 (5)	0.0044 (15) [−10. (13)]	0.0042 (15) [−5. (13)]	0.0039 (15) [3. (13)]
$(1/2)(\tilde{\varepsilon}_{ab} + \tilde{\varepsilon}_{ba})' = d'$	0.0065 (8)	0.0060 (22) [8. (12)]	0.0061 (22) [6. (12)]	0.0064 (22) [2. (12)]
$(1/2)(\tilde{\varepsilon}_{bc} + \tilde{\varepsilon}_{cb})' = c'$	—	−0.0024	−0.0023	−0.0021
$(1/2)(\tilde{\varepsilon}_{ac} + \tilde{\varepsilon}_{ca})' = e'$	—	−0.0043	−0.0042	−0.0045
$\lvert\mu_a/\mu_b\rvert$[b]	0.400	0.030	0.0625	0.153
$\lvert\mu_c/\mu_b\rvert$[b]	0.914	0.940	0.922	0.949
T_{00}	7501.2532 (3)	7476.6452 [0.33]	7020.2903 [6.41]	7572.9013 [0.96]

[a] Fit temperature of 15.0 K. [b] Determined from fit values of $\theta = 68.2^\circ$, $\phi = 49.7^\circ$.

all 15 molecular parameters incorporated in $\mathscr{H}_T$ for the $\tilde{A}$ and $\tilde{X}$ states are well determined.

Rather striking is the fact that the experimental precision of the parameters for the G_1G_2 conformer of propyl peroxy is very comparable to that which we previously reported for CD_3O_2 and $C_2H_5O_2$. While this result is counterintuitive, we expect the high precision obtained in this spectral fit to be attributable to the fact that the EA approach uses both the (somewhat less precise) frequencies for the propyl peroxy transitions *and* the intensity information contained in the $C_3H_7O_2$ spectrum, while the LSF method used only the transition frequency information for CD_3O_2. Since CRDS is an absorption-based technique, even absolute intensities are reliable, and the EA approach is ideal for fitting even highly congested CRDS spectra.

Once we have the experimental results of Table 1 we can use them to benchmark the results of various electronic structure calculations that are also given in Table 1. It appears that the MP2(FULL) method with a 6-31g(d) basis set reproduces extremely well the rotational constants for both the $\tilde{A}$ and $\tilde{X}$ states (within 0.4%) which is consistent with the observations made in our study of the ethyl peroxy radical.[28] As expected, the CCSD method also reproduces the rotational constants well but not as well as the MP2(FULL) method, the geometry optimization step of the G2 compound method.[49] Finally, the DFT method provides the least precise rotational constants.

Having found that MP2(FULL) provides an economical method to calculate accurate rotational constants, we have used it to calculate them for all 7 conformers of the two propyl peroxy isomers. These results are shown in Table 2. Comparison of these values with the experimental rotational constants of Table 1 confirms unambiguously the assignment of the analyzed sub-band to the G_1G_2 conformer of 1-propyl peroxy.

Table 2 Calculated rotational constants of the optimized equilibrium geometry for all conformers of the propyl peroxy radical for both the ground and first excited electronic state. The calculations were performed at the MP2(FULL) level with a 6-31g(d) basis set

	$G'_1\ G_2$	T_1T_2	T_1G_2	G_1T_2	G_1G_2	Iso G	Iso T
A″	0.28704	0.76639	0.42831	0.50935	0.32174	0.22300	0.26572
B″	0.12454	0.07323	0.09283	0.08420	0.10809	0.15540	0.13718
C″	0.09724	0.06945	0.08350	0.079247	0.10040	0.11791	0.09979
A′	0.27287	0.72583	0.43610	0.48144	0.30243	0.21828	0.26403
B′	0.12875	0.07389	0.09206	0.08538	0.11137	0.15319	0.13729
C′	0.09694	0.06969	0.08312	0.07931	0.10286	0.11789	0.09961

If one looks at the different components of the spin-rotation tensor, we can easily see from Table 1 that these constants are generally in good agreement with the predictions made using the semi-empirical method described in section 5. As for the rotational constants, the MP2(FULL) method provides the most accurate estimate. The discrepancy among the calculated values is fairly easy to understand. Since the prediction of the spin-rotation tensor depends upon the optimized geometry of the molecule, it becomes obvious that the MP2(FULL) geometry would provide the best estimate of the spin-rotation constants while the B3LYP will provide the lowest performance, just as we found for the rotational constants.

As Table 1 shows we actually only used the real part of the spin-rotation tensor to fit our spectrum. This result is partially predicated upon practicality. The EA program has not been adapted to diagonalize a complex $\mathscr{H}_T$ matrix. However, this approximation was justified by using our SpecView program[39] which can handle complex matrices. By adding the estimated values for c and e from the MP2(FULL) prediction into $\mathscr{H}_T$ and by examining the resulting predicted spectrum from SpecView the largest shift in frequency is found to be $\approx$ 4.0 MHz, which,

at our resolution, is not significant. This approximation is further confirmed by comparing simulations including, or not, the two extra imaginary components of the spin-rotation tensor.

Since the G_1G_2 conformer of the propyl peroxy radical has C_1 symmetry, non-vanishing components of the transition dipole moment lie along all three axes, a, b and c. The calculated and experimental results can be found in Table 1. One can observe a somewhat larger discrepancy between experiment and calculations for the relative components of the transition dipole than for the $\tilde{A}$ and $\tilde{X}$ state parameters. However, it is well known that transition dipoles are difficult to calculate and even more so for the intrinsically weak $\tilde{A}$–$\tilde{X}$ transition. The fairly significant variation of the calculated dipoles using the three different optimized geometries supports this supposition.

6.1.2 The G_1T_2 conformer of n-$C_3H_7O_2$. As mentioned previously, the G_1T_2 conformer of the n-propyl peroxy is estimated to be located about 27 cm^{-1} above the G_1G_2 conformer and a sub-band is observed near to the location of the unresolved band in the room-temperature spectra that is assigned to the G_1T_2 conformer (as shown in Fig. 3). The spectrum spreads over $\approx$10 cm^{-1} with a signal to noise ratio of about 20 : 1 for the strongest bands. We have performed a similar analysis on this band as the one for the band of the G_1G_2 conformer. The parameters resulting from the EA analysis of this sub-band are given in Table 3. The rotational temperature has been fitted to be $\approx$18 K (k_BT_R = 12.51 cm^{-1}). It is clear that the simulation is in perfect agreement with the experimental spectrum. By comparing the experimental molecular parameters with the calculated and predicted ones in Table 3, we came to the same conclusion as for the G_1G_2 conformer, *i.e.* that the MP2(FULL) is suitable to make the best predictions for molecular parameters and that the B3LYP method gives the poorest agreement of the three methods employed. By comparing the calculated rotational constants in Table 2 with the experimental values in Table 3, it is clear that the assignment of this band to the G_1T_2 conformer is correct.

It is of interest to compare the present highly accurate values of T_{00} = 7501.2532(3) and 7576.2469(4) cm^{-1} for the G_1G_2 and G_1T_2 conformers, respectively, with the values of 7508(2) and 7569(2) cm^{-1} from the room-temperature spectra.[14,20] It is somewhat surprising to see discrepancies significantly beyond the estimated experimental measurement error in the room-temperature experiments. This result is particularly striking since our recently reported T_{00} values from jet-cooled spectra agreed to well within the room-temperature experimental error for CD_3O_2,[27] and both the G and T conformers of ethyl peroxy.[28] However, in these cases, the room-temperature bands, while unresolved, were isolated. In the case of the G_1G_2 and GT_2 conformers of 1-propyl peroxy, the room-temperature bands are significantly overlapped and this may well explain the discrepancies.

It also is interesting to compare the present experimental results with the calculated excitation energy, T_{00}, for the electronic structure methods which are summarized in Table 1 and 3. The energy separation for the MP2(FULL) was obtained by calculating both electronic states using the G2 compound method which already contains the ZPE correction as well as several higher order energy correction terms. The energies obtained for the CCSD and B3LYP energies have been corrected by the ZPE correction under the harmonic oscillator approximation. In the former case, an average of the B3LYP and G2 ZPE (which differ by $\approx$10 cm^{-1}) energies was used. It is no surprise that the MP2(FULL) calculation is the most accurate one as pointed out by Sharp *et al.*[20] On the other hand, it is surprising that the CCSD calculation is less accurate than the DFT one since its global minimum structure of the radical appears to be more accurate than the B3LYP-DFT calculation.

6.2 The G conformer of the 2-propyl peroxy radical isomer

The 2-propyl peroxy isomer is known to have only 2 conformers, as show in Fig. 1. It has been calculated[15] that the G conformer is the most stable and that the T conformer lies about 149 cm^{-1} higher. So it is likely that under jet-cooled conditions, one should only observe the G conformer. The only band observed for isopropyl peroxy is illustrated in Fig. 4. The signal to noise ratio appears to be excellent in this spectrum (more than 120 : 1 for the strongest feature) and the spectrum spreads over $\approx$10 cm^{-1}. However, the experimental spectrum of the iso-propyl peroxy isomer exhibits less well resolved rotational and spin-rotational structures than does the n-propyl peroxy isomer, which makes the EA approach even more important for analyzing the former spectra.

We have employed the same approach as described above for the analysis of 1-propyl isomer. The results are summarized in Table 4 and Fig. 4. The rotational temperature was found to be 13.3 K (k_BT_R = 9.24 cm^{-1}). When looking at the top insert of Fig. 4, one can see that discrepancies between the simulation and the experimental spectrum are essentially non-existent. Moreover, there is extremely good agreement between the fitted molecular parameters and the calculated and predicted ones using the MP2(FULL) method.

Comparison between the experimental rotational constants in Table 4 and the calculated ones in Table 2 confirm the room-temperature assignment of this band to the G conformer of isopropyl peroxy. The highly accurate value of T_{00} = 7568.0950(2) agrees well with the room-temperature value[14,20] of 7567(2) given the latter's experimental error. The good agreement here, compared to the poorer agreement for the n-propyl peroxy conformers, likely reflects the fact that while the room-temperature band is unresolved, it is isolated for the isopropyl peroxy isomer. Referring to Table 4, we see that the G2 calculation using the MP2(FULL) result, is by far the closest to experiment.

7. Conclusion

We have successfully recorded the partially rotationally resolved spectra of several isomers and conformers of the propyl peroxy radical, $C_3H_7O_2$, *i.e.* the G_1G_2 and G_1T_2 conformers of the n-propyl peroxy and the G conformer of iso-propyl peroxy. We have used an EA approach to analyze the observed spectra. This approach allowed us to obtain an excellent match between the simulated and the experimental

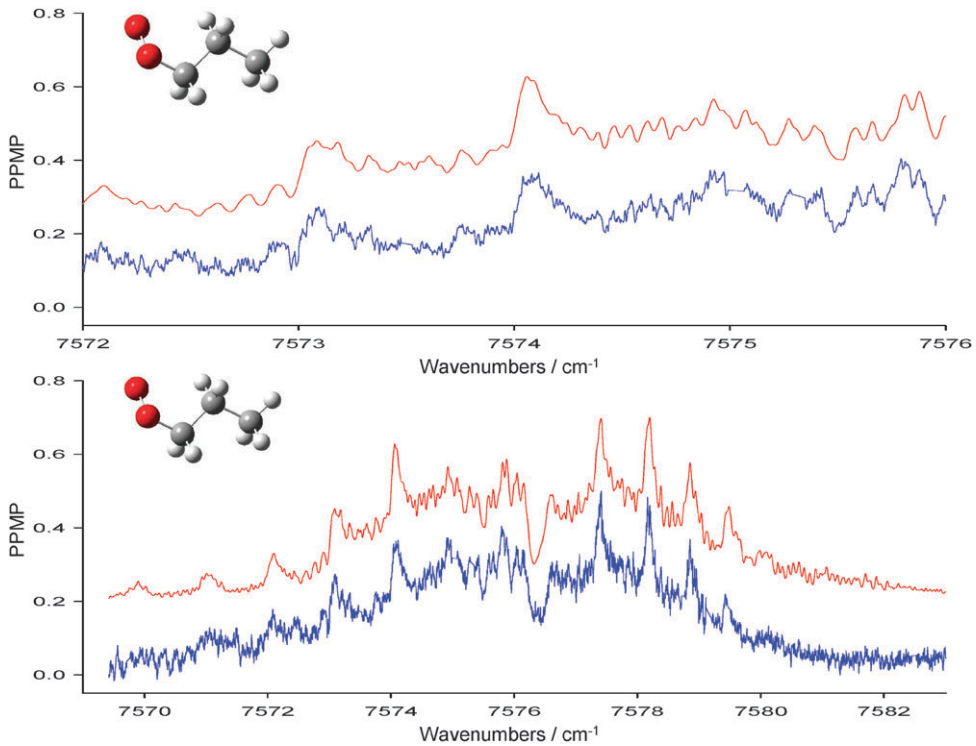

Fig. 3 Experimental and simulated spectra of the G_1T_2 conformer of the n-$C_3H_7O_2$ radical. The upper panel shows an enlargement of a 4 cm^{-1} section of the lower panel. In each panel, the top red trace is the simulated spectrum, using the fitted constants in Table 3, shifted upward by 0.2 PPMP while the bottom blue trace is the experimental spectrum. Axis conventions are the same as Fig. 2.

Table 3 Molecular parameters of G_1T_2 conformer of n-$C_3H_7O_2$ radical from the experimental spectrum and from the indicated electronic structure calculations (see text for details). The calculated T_{00} have been corrected by the scaled[49] ZPE correction under the harmonic oscillator assumption. The numbers in square brackets represent the percentage of error of the predicted constant with respect to the fitted results. The calculated and predicted constants are for the equilibrium geometry. The components of the transition moment are computed using the CIS method using the optimized geometries indicated

Const./cm^{-1}	Fit[a]	MP2(FULL)\6-31+g(d)	CCSD\6-31+g(d)	B3LYP\6-31+g(d)
A''	0.50544 (4)	0.50935 [−0.774 (8)]	0.50192 [0.696 (8)]	0.51277 [−1.450 (8)]
B''	0.08389 (2)	0.08420 [−0.370 (24)]	0.08345 [0.524 (24)]	0.08185 [2.432 (24)]
C''	0.07905 (2)	0.07925 [−0.253 (25)]	0.07843 [0.784 (25)]	0.07745 [2.024 (25)]
$\tilde{\varepsilon}_{aa}'' = -(a_0 + 2a)''$	−0.0106 (7)	−0.0118 (15) [−11. (7)]	−0.0117 (15) [−10. (7)]	−0.0125 (15) [−18. (7)]
$\tilde{\varepsilon}_{bb}'' = (a + b - a_0)''$	−0.0037 (3)	−0.0035 (14) [5. (8)]	−0.0035 (14) [5. (8)]	−0.0032 (14) [14. (8)]
$\tilde{\varepsilon}_{cc}'' = (a - b - a_0)''$	−0.0025 (3)	−0.0016 (15) [36. (12)]	−0.0016 (15) [36. (12)]	−0.0017 (15) [36. (12)]
$(1/2)(\tilde{\varepsilon}_{ab} + \tilde{\varepsilon}_{ba})'' = d''$	−0.0021 (33)	−0.0049 (22) [−133. (157)]	−0.0049 (22) [−133. (157)]	−0.0053 (22) [−152. (157)]
$(1/2)(\tilde{\varepsilon}_{bc} + \tilde{\varepsilon}_{cb})'' = c''$	—	0.0020	0.0020	0.0020
$(1/2)(\tilde{\varepsilon}_{ac} + \tilde{\varepsilon}_{ca})'' = e''$	—	0.0006	0.0006	0.0010
A'	0.47968 (4)	0.48144 [−0.367 (8)]	0.47526 [0.921 (8)]	0.48692 [−1.509 (8)]
B'	0.08518 (2)	0.08538 [−0.235 (23)]	0.08453 [0.763 (23)]	0.08306 [2.489 (23)]
C'	0.07899 (2)	0.07931 [−0.405 (25)]	0.07838 [0.772 (25)]	0.07723 [2.228 (25)]
$\tilde{\varepsilon}_{aa}' = -(a_0 + 2a)'$	0.0104 (7)	0.0135 (15) [−30. (7)]	0.0137 (15) [−32. (7)]	0.0149 (15) [−43. (7)]
$\tilde{\varepsilon}_{bb}' = (a + b - a_0)'$	0.0037 (3)	0.0041 (14) [−11. (8)]	0.0040 (14) [−8. (8)]	0.0037 (14) [0. (8)]
$\tilde{\varepsilon}_{cc}' = (a - b - a_0)'$	0.0005 (3)	0.0004 (15) [20. (60)]	0.0003 (15) [40. (60)]	0.0004 (15) [20. (60)]
$(1/2)(\tilde{\varepsilon}_{ab} + \tilde{\varepsilon}_{ba})' = d'$	0.0092 (4)	0.0086 (22) [2. (4)]	0.0086 (22) [7. (4)]	0.0090 (22) [2. (4)]
$(1/2)(\tilde{\varepsilon}_{bc} + \tilde{\varepsilon}_{cb})' = c'$	—	−0.0020	−0.0020	−0.0019
$(1/2)(\tilde{\varepsilon}_{ac} + \tilde{\varepsilon}_{ca})' = e'$	—	−0.0007	−0.0007	−0.0009
$\lvert\mu_b/\mu_a\rvert^b$	0.735	0.495	0.540	0.554
$\lvert\mu_c/\mu_a\rvert^b$	0.711	0.462	0.460	0.386
T_{00}	7576.2469 (4)	7566.8709 [0.12]	7099.6110 [6.29]	7655.9997 [1.05]

[a] Fit temperature of 17.9 K. [b] Determined from fit values of $\theta = 36.3°$, $\phi = 60.2°$.

spectra producing a set of molecular parameters characterizing the $\tilde{X}$ and $\tilde{A}$ states of the radicals.

We have confirmed the conformer room-temperature assignments previously made by Tarczay *et al.*[15] which were made entirely based upon electronic structure calculations. Obtaining molecular parameters characterizing these radicals in both electronic states allowed us to benchmark quantum chemistry calculations by several different methods and basis

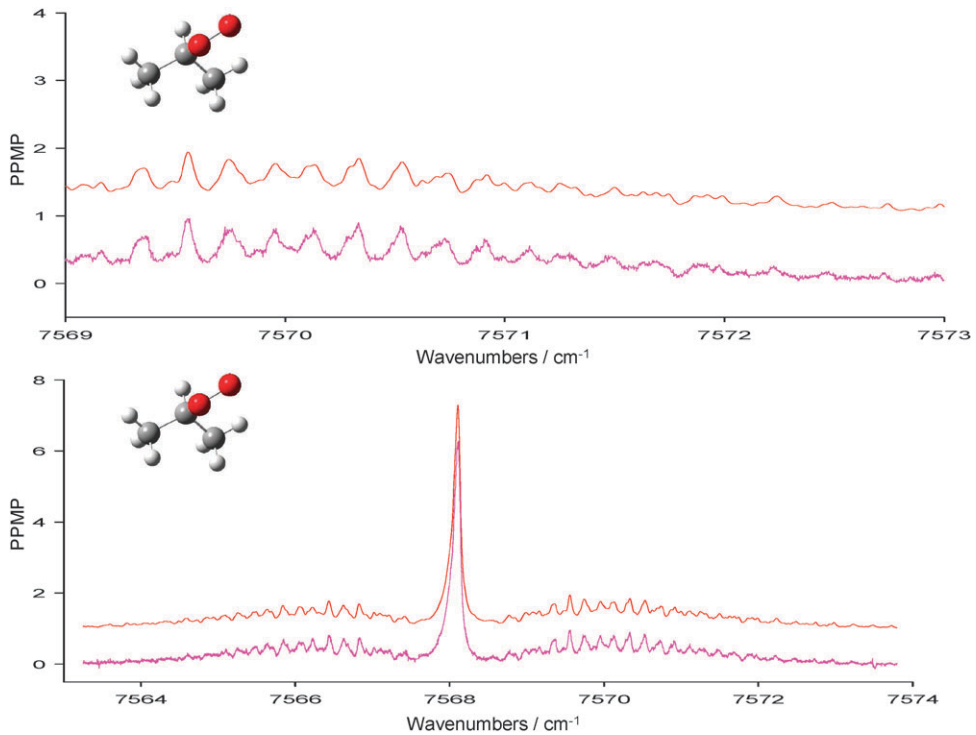

Fig. 4 Experimental and simulated spectra of the G conformer of the iso-$C_3H_7O_2$ radical. The upper panel shows an enlargement of a 4 cm^{-1} section of the lower panel. In each panel, the top red trace is the simulated spectrum, using the fitted constants in Table 4, shifted upward by 1 PPMP while the bottom magenta trace is the experimental spectrum. Axis conventions are the same as Fig. 2.

Table 4 Molecular parameters of the G conformer of iso-$C_3H_7O_2$ radical from the experimental spectrum and from the indicated electronic structure calculations (see text for details). The calculated T_{00} have been corrected by the scaled[49] ZPE correction under the harmonic oscillator assumption. The numbers in square brackets represent the percentage of error of the predicted constant with respect to the fitted results. The calculated and predicted constants are for the equilibrium geometry. The components of the transition moment are computed using the CIS method using the optimized geometries indicated

Const./cm^{-1}	Fit[a]	MP2(FULL)\6-31+g(d)	CCSD\6-31+g(d)	B3LYP\6-31+g(d)
A''	0.26527 (4)	0.26572 [−0.170 (15)]	0.26340 [0.705 (15)]	0.26162 [1.376 (15)]
B''	0.13692 (3)	0.13718 [−0.190 (22)]	0.13530 [1.183 (22)]	0.13408 [2.074 (22)]
C''	0.09916 (4)	0.09979 [−0.635 (40)]	0.09860 [0.565 (40)]	0.09772 [1.452 (40)]
$\tilde{\varepsilon}_{aa}'' = -(a_0 + 2a)''$	−0.0139 (7)	−0.0135 (15) [3. (5)]	−0.0134 (15) [4. (5)]	−0.0133 (15) [4.317 (5)]
$\tilde{\varepsilon}_{bb}'' = (a + b - a_0)''$	−0.0013 (5)	−0.0024 (14) [−84. (38)]	−0.0023 (14) [−77. (38)]	−0.0021 (14) [−62. (38)]
$\tilde{\varepsilon}_{cc}'' = (a - b - a_0)''$	−0.0012 (7)	−0.0017 (15) [−42. (58)]	−0.0017 (15) [−42. (58)]	−0.0018 (15) [−50. (58)]
$(1/2)(\tilde{\varepsilon}_{ab} + \tilde{\varepsilon}_{ba})'' = d''$	0.0128 (19)	0.0029 (22) [77. (15)]	0.0028 (22) [78. (15)]	0.0027 (22) [79. (15)]
$(1/2)(\tilde{\varepsilon}_{bc} + \tilde{\varepsilon}_{cb})'' = c''$	—	−0.0019	−0.0019	−0.0019
$(1/2)(\tilde{\varepsilon}_{ac} + \tilde{\varepsilon}_{ca})'' = e''$	—	−0.0025	−0.0025	−0.0026
A'	0.26406 (4)	0.26403 [0.011 (15)]	0.26241 [0.625 (15)]	0.26142 [1.000 (15)]
B'	0.13710 (3)	0.13729 [−0.139 (22)]	0.13519 [1.393 (22)]	0.13399 [2.268 (22)]
C'	0.09912 (4)	0.09961 [−0.494 (40)]	0.09827 [0.858 (40)]	0.09723 [1.907 (40)]
$\tilde{\varepsilon}_{aa}' = -(a_0 + 2a)'$	0.0172 (7)	0.0184 (15) [−7. (4)]	0.0184 (15) [−7. (4)]	0.0185 (15) [−8. (4)]
$\tilde{\varepsilon}_{bb}' = (a + b - a_0)'$	0.0013 (5)	0.0010 (14) [23. (38)]	0.0010 (14) [23. (38)]	0.0010 (14) [23. (38)]
$\tilde{\varepsilon}_{cc}' = (a - b - a_0)'$	0.0004 (7)	0.0003 (15) [25. (175)]	0.0003 (15) [25. (175)]	0.0002 (15) [50. (175)]
$(1/2)(\tilde{\varepsilon}_{ab} + \tilde{\varepsilon}_{ba})' = d'$	−0.0018 (50)	−0.0031 (22) [−72. (276)]	−0.0030 (22) [−67. (276)]	−0.0030 (22) [267 (276)]
$(1/2)(\tilde{\varepsilon}_{bc} + \tilde{\varepsilon}_{cb})' = c'$	—	−0.0018	−0.0018	0.0017
$(1/2)(\tilde{\varepsilon}_{ac} + \tilde{\varepsilon}_{ca})' = e'$	—	0.0020	0.0019	0.0017
$\lvert\mu_b/\mu_a\rvert^b$	0.024	0.515	0.523	0.413
$\lvert\mu_c/\mu_a\rvert^b$	0.876	0.697	0.646	0.587
T_{00}	7568.0950 (4)	7566.2345 [0.02]	7124.1834 [5.87]	7662.2373 [1.24]

[a] Fit temperature of 13.3 K. [b] Determined from fit values of $\theta = 1.4°$, $\phi = 48.8°$.

sets. We also demonstrated that by following the formalism of Brown, Sears and Watson[38] and extended by Tarczay *et al.*,[47] one is able to predict the different components of the spin-rotation tensors rather well. Finally, this work confirms the effectiveness of using an EA approach to simulate spectra with varying degrees of resolution.

Acknowledgements

The authors gratefully acknowledge the support of the US National Science Foundation via grant CHE-0511809 and the Ohio Supercomputer Center.

References

1 P. D. Lightfoot, R. A. Cox, J. N. Crowley, M. Destriau, G. D. Hayman, M. E. Jenkin, G. K. Moortgat and F. Zabel, *Atmos. Environ., Part A*, 1992, **26**, 1805.
2 G. S. Tyndall, R. A. Cox, C. Granier, R. Lesclaux, G. K. Moortgat, M. J. Pilling, A. R. Ravishankara and T. J. Wallington, *J. Geophys. Res.*, 2001, **106**, 12157.
3 M. J. Pilling, in *Chemical Kinetics Low-Temperature Combustion and Autoignition*, Elsevier, Amsterdam, 1997, vol. 35.
4 T. J. Wallington and O. J. Nielsen, in *Peroxyl Radicals*, John Wiley and Sons, New York, 1997, p. 457.
5 G. J. Frost, G. B. Ellison and V. Vaida, *J. Phys. Chem. A*, 1999, **103**, 10169.
6 H. J. Curran, P. Gaffuri, W. J. Pitz and C. K. Westbrook, *Combust. Flame*, 1998, **114**, 149.
7 H.-H. Carstensen, C. V. Naik and A. M. Dean, *J. Phys. Chem. A*, 2005, **109**, 2264.
8 T. A. Miller, *Mol. Phys.*, 2006, **104**, 2581.
9 T. J. Wallington, P. Dagaut and M. J. Kurylo, *Chem. Rev.*, 1992, **92**, 667.
10 J. A. Jafri and D. H. Phillips, *J. Am. Chem. Soc.*, 1990, **112**, 2586.
11 O. J. Nielsen and T. J. Wallington, in *Peroxyl Radicals*, John Wiley and Sons, New York, NY, 1997, ch. Ultraviolet Absorption Spectra of Peroxy Radicals in the Gas Phase, p. 69.
12 H. E. Hunziker and H. R. Wendt, *J. Chem. Phys.*, 1976, **64**, 3488.
13 M. B. Pushkarsky, S. J. Zalyubovsky and T. A. Miller, *J. Chem. Phys.*, 2000, **112**, 10695.
14 S. J. Zalyubovsky, B. G. Glover, T. A. Miller, C. Hayes, J. K. Merle and C. M. Hadad, *J. Phys. Chem. A*, 2005, **109**, 1308.
15 G. Tarczay, S. J. Zalyubovsky and T. A. Miller, *Chem. Phys. Lett.*, 2005, **406**, 81.
16 B. G. Glover and T. A. Miller, *J. Phys. Chem. A*, 2005, **109**, 11191.
17 P. Rupper, E. N. Sharp, G. Tarczay and T. A. Miller, *J. Phys. Chem. A*, 2007, **111**, 832.
18 C.-Y. Chung, C.-W. Cheng, Y.-P. Lee, H.-Y. Liao, E. N. Sharp, P. Rupper and T. A. Miller, *J. Chem. Phys.*, 2007, **127**, 044311.
19 E. N. Sharp, P. Rupper and T. A. Miller, *J. Phys. Chem. A*, 2008, **112**, 1445.
20 E. N. Sharp, P. Rupper and T. A. Miller, *Phys. Chem. Chem. Phys.*, 2008, **10**, 3955.
21 S. J. Blanksby, T. M. Ramond, G. E. Davico, M. R. Nimlos, S. Kato, V. M. Bierbaum, W. C. Lineberger, G. B. Ellison and M. Okumura, *J. Am. Chem. Soc.*, 2001, **123**, 9585.
22 G. Meloni, P. Zou, S. J. Klippenstein, M. Ahmed, S. R. Leoni, C. A. Taatjes and D. L. Osborn, *J. Am. Chem. Soc.*, 2006, **128**, 13559.
23 D. B. Atkinson and J. L. Spillman, *J. Phys. Chem. A*, 2002, **106**, 8891.
24 H. B. Fu, Y. J. Hu and E. R. Bernstein, *J. Chem. Phys.*, 2006, **125**, 014310.
25 P. Dupré and T. A. Miller, *Rev. Sci. Instrum.*, 2007, **78**, 033102.
26 S. Wu, P. Dupré and T. A. Miller, *Phys. Chem. Chem. Phys.*, 2006, **8**, 1682.
27 S. Wu, P. Dupré, P. Rupper and T. A. Miller, *J. Chem. Phys.*, 2007, **127**, 224305.
28 G. M. P. Just, P. Rupper, T. A. Miller and W. L. Meerts, *J. Chem. Phys.*, 2009, **131**, 184303.
29 L. S. Rothman, D. Jacquemart, A. Barbe, D. C. Benner, M. Birk, L. R. Brown, M. R. Carleer, C. Chackerian, J. K. Chance, L. H. Coudert, V. Dana, V. M. Devi, J. M. Flaud, R. R. Gamache, A. Goldman, J. M. Hartmann, K. W. Jucks, A. G. Maki, J. Y. Mandin, S. T. Massie, J. Orphal, A. Perrin, C. P. Rinsland, M. A. H. Smith, J. Tennyson, R. N. Tolchenov, R. A. Toth, J. V. Auwera, P. Varanasi and G. Wagner, *J. Quant. Spectrosc. Radiat. Transfer*, 2005, **96**, 139.
30 S. Gopalakrishnan, C. C. Carter, L. Zu, V. Stakhursky, G. Tarczay and T. A. Miller, *J. Chem. Phys.*, 2003, **118**, 4954.
31 R. N. Zare, in *Angular Momentum*, Wiley Interscience, New York, NY, 1988.
32 J. H. V. Vleck, *Rev. Mod. Phys.*, 1951, **23**, 213.
33 W. T. Raynes, *J. Chem. Phys.*, 1964, **41**, 3020.
34 R. F. Curl and J. L. Kinsey, *J. Chem. Phys.*, 1961, **35**, 1758.
35 A. Carrington and B. J. Howard, *Mol. Phys.*, 1970, **18**, 225.
36 X. Q. Tan, J. M. Williamson, S. C. Foster and T. A. Miller, *J. Phys. Chem.*, 1993, **97**, 9311.
37 J. M. Brown and T. J. Sears, *J. Mol. Spectrosc.*, 1979, **75**, 111.
38 J. M. Brown, T. J. Sears and J. K. G. Watson, *Mol. Phys.*, 1980, **41**, 173.
39 V. L. Stakhursky and T. A. Miller, *56th OSU International Symposium on Molecular Spectroscopy*, The Ohio State University, Columbus, 2001, vol. TC06, p. 107.
40 W. L. Meerts and M. Schmitt, *Int. Rev. Phys. Chem.*, 2006, **25**, 353.
41 N. Hansen and A. Ostenmeier, *Evol. Comput.*, 2001, **9**, 159.
42 A. Ostenmeier, A. Gawelcyk and N. Hansen, in *Parallel Problem Solving from Nature, PPSN III*, Springer, Berlin/Heidelberg, 1994, vol. 3.
43 I. Kalkman, C. Vu, M. Schmitt and W. L. Meerts, *ChemPhysChem*, 2008, **9**, 1788.
44 I. Kalkman, C. Brand, T.-B. C. Vu, W. L. Meerts, Y. N. Svartsov, O. Dopfer, K. Mueller-Dethlefs, S. Grimme and M. Schmitt, *J. Chem. Phys.*, 2009, **130**, 224303.
45 J. A. Hageman, R. Wehrens, R. de Gelder, W. L. Meerts and L. M. C. Buydens, *J. Chem. Phys.*, 2000, **113**, 7955.
46 M. J. Frisch, G. W. Trucks, H. B. Schlegel, G. E. Scuseria, M. A. Robb, J. R. Cheeseman, J. A. Montgomery, Jr., T. Vreven, K. N. Kudin, J. C. Burant, J. M. Millam, S. S. Iyengar, J. Tomasi, V. Barone, B. Mennucci, M. Cossi, G. Scalmani, N. Rega, G. A. Petersson, H. Nakatsuji, M. Hada, M. Ehara, K. Toyota, R. Fukuda, J. Hasegawa, M. Ishida, T. Nakajima, Y. Honda, O. Kitao, H. Nakai, M. Klene, X. Li, J. E. Knox, H. P. Hratchian, J. B. Cross, V. Bakken, C. Adamo, J. Jaramillo, R. Gomperts, R. E. Stratmann, O. Yazyev, A. J. Austin, R. Cammi, C. Pomelli, J. Ochterski, P. Y. Ayala, K. Morokuma, G. A. Voth, P. Salvador, J. J. Dannenberg, V. G. Zakrzewski, S. Dapprich, A. D. Daniels, M. C. Strain, O. Farkas, D. K. Malick, A. D. Rabuck, K. Raghavachari, J. B. Foresman, J. V. Ortiz, Q. Cui, A. G. Baboul, S. Clifford, J. Cioslowski, B. B. Stefanov, G. Liu, A. Liashenko, P. Piskorz, I. Komaromi, R. L. Martin, D. J. Fox, T. Keith, M. A. Al-Laham, C. Y. Peng, A. Nanayakkara, M. Challacombe, P. M. W. Gill, B. G. Johnson, W. Chen, M. W. Wong, C. Gonzalez and J. A. Pople, *GAUSSIAN 03 (Revision C.02)*, Gaussian, Inc., Wallingford, CT, 2004.
47 G. Tarczay, S. Gopalakrishnan and T. A. Miller, *J. Mol. Spectrosc.*, 2003, **220**, 276.
48 S. Gopalakrishnan, L. Zu and T. A. Miller, *J. Phys. Chem. A*, 2003, **107**, 5189.
49 J. B. Foresman and Æ. Frisch, in *Exploring Chemistry with Electronic Structure Methods*, Gaussian, Inc., Pittsburgh, PA, 2nd edn, 1996.

